Journal of Molecular Liquids 312 (2020) 113293

Contents lists available at ScienceDirect

Journal of Molecular Liquids

journal homepage: www.elsevier.com/locate/molliq

The influence of polydispersity on the structural properties of the isotropic phase of magnetic nanoplatelets☆

Margaret Rosenberg [a,*], Žiga Gregorin [b], Patricija Hribar Boštjančič [b,c], Nerea Sebastián [b], Darja Lisjak [b], Sofia S. Kantorovich [a,d], Alenka Mertelj [b], Pedro A. Sánchez [d,e]

[a] Faculty of Physics, University of Vienna, Boltzmanngasse 5, 1090 Vienna, Austria
[b] Jožef Stefan Institute, Jamova Cesta 39, 1000 Ljubljana, Slovenia
[c] Jožef Stefan International Postgraduate School, Jamova cesta 39, 1000 Ljubljana, Slovenia
[d] Ural Federal University, Lenin Av. 51, Ekaterinburg 620000, Russian Federation
[e] Wolfgang Pauli Institute, c/o Faculty of Mathematics, University of Vienna, Oskar-Morgenstern-Platz 1, 1090 Vienna, Austria

ARTICLE INFO

Article history:
Received 24 February 2020
Received in revised form 20 April 2020
Accepted 3 May 2020
Available online 19 May 2020

Keywords:
Magnetic platelets
Static structure factor
Molecular dynamics

ABSTRACT

By employing a combination of Molecular Dynamics simulations and experimental SAXS studies, we investigate low-concentration suspensions of polydisperse magnetic platelets with dipole moments perpendicular to the platelets' plane. Exploiting the precise control of platelet size and shape in simulation, we are also able to contrast these results with equivalent density monodisperse suspensions. We show how the polydispersity may lead to the reduction of the orientational and spatial correlations in the absence of an applied field, while simultaneously facilitating the field-induced transition into a nematic-like phase. Along with structural properties, we investigate the magnetic response. This allows us to confirm that the inter-platelet magnetic correlations have a negligible influence on the structure of the low-density suspensions.

1. Introduction

Magnetically responsive liquids are very appealing for a wide range of applications, as demonstrated by their extensive use in magnetic dampers and seals, biomedicine [1], vibratory energy harvesting [2–5], magneto-mechanical actuation and pumping in micro-magnetofluidics [6,7], magnetic control of light [8,9], targeted drug delivery [9,10] or magnetic field sensing and visualisation [11]. The unique properties of magnetically responsive liquids give rise to an astonishing versatility of applications, yet make the fundamental understanding of such systems rather challenging.

Although there is no fundamental reason opposing spontaneous macroscopic polar ordering, either ferroelectric or ferromagnetic, in liquids, examples of such ordering are scarce and mostly limited to conventional molecular liquid crystals where polar order is accompanied by partial positional order [12]. In conventional magnetic fluids, also known as ferrofluids – suspensions of spherical single-domain magnetic nanoparticles [13] – no ferromagnetic ordering is observed, despite an extensive active search [14–27], due to the strong anisotropy of the interparticle dipolar interactions.

At the end of the 20th century, the systems of dipolar particles with additional shape anisotropy (anisometry) attracted a lot of attention from theoreticians due to their ability to form various liquid-crystalline phases, be that nematic, antiferroelectric nematic, smectic, *etc.* [28–41], which was later revisited in the works [42–44]. The main focus of the later studies was on hard/soft ellipsoids or spherocylinders, with point dipole moments coaligned along the main axis, which typically corresponds to the axis of revolution. Systems of anisometric dipolar particles can undergo a vapour-liquid phase transition [45], in contrast to dipolar hard-sphere systems in which this transition has never been found [46,47]. Even systems with higher order moments were investigated, albeit less frequently [41].

Anisometric particles with the dipole moment oriented orthogonally to their main axis were not addressed as actively [48–53] as the systems discussed above. However, this route of study has led to the discovery of new crystalline phases. Recently, haematite colloids have attracted the interest of multiple experimental groups, as their magnetic moments are aligned along the short axis [54,55]. In general, the positioning of the dipole inside the ellipsoid can be more complex [56].

The oblate spheroidal shape referred to as "platelet" is one of the most recent types of anisometric shapes introduced in the synthesis of magnetic and non-magnetic nanoparticles. It has been experimentally

☆ The special issue article has been accepted for publication under the special issue "CPBCI 2019".

* Corresponding author.
E-mail address: margaret.rosenberg@univie.ac.at (M. Rosenberg).

https://doi.org/10.1016/j.molliq.2020.113293

proven that discotic nematic ordering can appear in suspensions of non-magnetic nanoplatelets above a threshold concentration, mainly determined by the shape anisotropy and the electrostatic interaction [57–59].

It was not until recently that experimental realisation of spontaneous ferromagnetic order in liquid was achieved in a system of scandium-substituted barium hexaferrite (Sc-BaHF) magnetic platelets in n-butanol [60]. While for low volume fractions only strong magnetic-field induced ordering is observed, above a certain threshold concentration nematic ordering of the platelets is promoted, resulting in a macroscopic magnetisation. In contrast to ferrofluids made of spherical particles, the combination of shape anisotropy, screened electrostatic and magnetic interactions between the platelets results their in positional and orientational correlations and promotes ferromagnetic ordering. This is a simplified picture and for a full description, long-range magnetic many body interactions need to be considered [61]. One of the remarkable observations for these systems is the formation of closed magnetic domains structures in thin rectangular capillaries and under zero-field conditions, which are textbook examples for soft ferromagnets [62]. The theory of such platelets was barely investigated, not only due to their recent synthesis, but also due to the complexity of interactions and parameters involved. Moreover, such platelets are polydisperse, which additionally makes the effects observed in these systems dependent on the granulometry.

This paper aims at putting forward a minimal simulation model of magnetic nanoplatelets (MPL). On its basis, we investigate the impact of platelets' polydispersity on the structural properties of the suspension below the isotropic-nematic transition, in which reorientation of particles can be caused by an applied magnetic field. The advantage of the simulation approach is that one can study a purely monodisperse system not accessible in experiment, then compare it to and contrast it with the polydisperse system.

The structure of our manuscript is as follows. In Section 2 we describe the experimental system. Subsequently, we introduce the simulation model and general simulation approach. The Result and Discussion section is subdivided into two parts. First, we explore the intrinsic equilibrium properties of the platelet suspension, comparing RDFs, bond order parameters and isotropic structure factors for monodisperse systems to those obtained for a polydisperse system with the experimentally observed size distribution. In the second part of the section, we discuss the influence of an applied homogeneous magnetic field on the aforementioned structural properties, while performing a critical analysis of polydispersity's impact. The impact of the latter is also elucidated in terms of magnetisation curves.

2. Experimental

Hydrothermal synthesis of BaHF results in a broad or bimodal particle size distribution [63], with too large particles, not suitable for stable suspensions. However, by partial substitution of Fe^{3+} with the more voluminous atoms Sc^{3+}, particle growth rate is decreased, achieving narrowed and monomodal particle size distribution [64] as shown in Fig. 1(a). Scandium substituted BaHF were synthesized hydrothermally and suspended in n-butanol using the surfactant dodecylbenzenesulfonic acid (DBSA). The thickness of the platelets was around 3.5 nm and the diameter distribution approximately log-normal (mean diameter of 55 nm and 20 nm deviation). Due to the strong magnetocrystalline anisotropy of the BaHF platelets, they exhibit magnetic dipole moments perpendicular to their plane. The magnetisation of the platelets was measured using a vibrating sample magnetometer (Lakeshore 7400 Series VSM) to be $2 \cdot 10^{-18}$ Am^2, which results in strong magnetic interparticle interactions. A typical transmission electron microscopy image of an experimental system of MPLs is presented in Fig. 1(b).

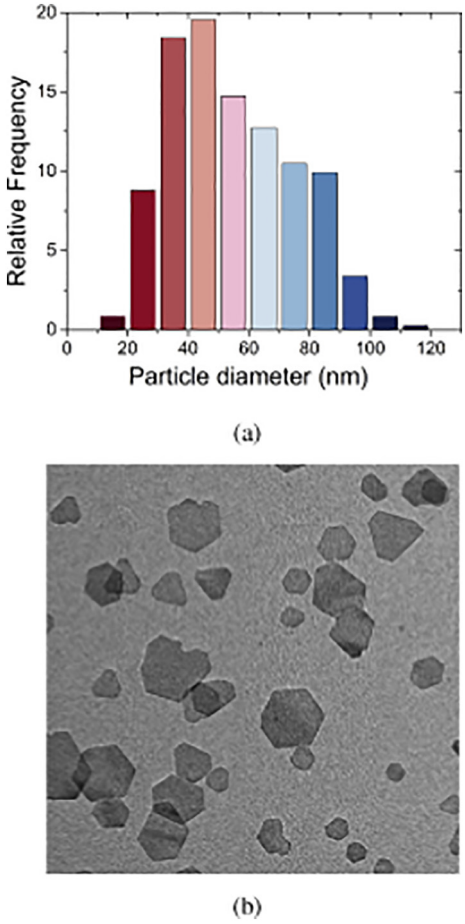

Fig. 1. (a) A typical MPL particle main diameter distribution obtained in the experiment; (b) TEM image of Sc-BaHF MPL.

3. Simulation

We put forward a coarse-grained approach to model MPL, and use Molecular Dynamics computer simulations in order to investigate mono- and polydisperse MPL systems, both in the absence of and in presence of an applied magnetic field.

3.1. MPL model

In order to simplify the calculations of MPL steric repulsion, while preserving the shape anisometry, we use a so-called “raspberry” representation. In this approach, a solid particle with a given shape is modelled as a rigid arrangement of smaller spheres, referred to as raspberry beads, distributed inside the volume boundary (see Fig. 2). By assigning proper interactions to every raspberry bead, one can model excluded volume effects in a discretised approximation. As the simulation particle can only move as a whole, the equations of motion need only be integrated for the central sphere, meaning that the raspberry beads are by far computationally cheaper than a typical simulation particle. In this work, the platelet shape is achieved by using Vogel's Algorithm to optimally distribute the raspberry bead centres on a disc. These beads each have a diameter of $\sigma = 1$, making the overall height of the platelet 1 in simulation units. This fast and efficient method allows to easily change the number of beads per platelet and as such to model mono- and poly-disperse systems without changing the surface properties of the platelets. In our approach, raspberry beads of different platelets repel each other according to Weeks-Chandler-Andersen potential [65]:

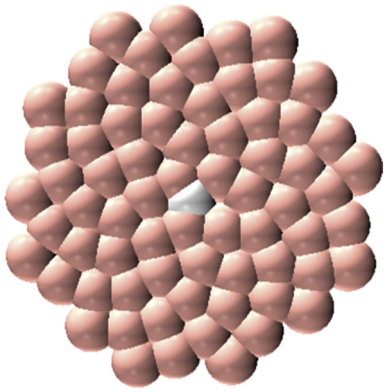

Fig. 2. Raspberry model of a platelet. The central bead (white) carries the dipole moment perpendicular to the page plane, pink beads are raspberry beads, each of which carries a charge q as described in the main text and a steric WCA repulsion according to Eq. (1). All beads have a diameter $\sigma = 1$.

$$\beta U_{WCA}(r) = \begin{cases} 4\varepsilon\left[\left(\frac{\sigma}{r}\right)^{12} - \left(\frac{\sigma}{r}\right)^{6} + \frac{1}{4}\right], r \le r_c 0, r \ge r_c \end{cases} \quad (1)$$

where r is the distance between the bead centres, with a cut-off distance $r_c = 2^{1/6}\sigma$, ε is the repulsion energy scale and the Boltzmann factor $\beta = 1/k_BT$, with T denoting temperature and k_B – the Boltzmann constant.

Electric charges and/or point magnetic dipoles can be assigned to any selection of raspberry elements in order to mimic distributions of surface charges and magnetic moments. We chose to assign magnetic dipoles only to central particles, and align them perpendicular to the platelet surface. This point-dipole approximation is efficient and, due to the electrostatic repulsion between platelets not allowing them to approach closely, should not introduce significant errors. The direction of the magnetic moment direction is fixed, whereas its absolute value $\mu(n)$ is scaled with the volume of the platelet magnetic core $v(n)$, such that $\mu(v(n)) = \mu_r \pi r^2 h$, where the constant μ_r is fixed such that the median platelet has a magnetic moment of 1 in simulation units. As a result, two random platelets with m and n raspberry beads, whose centres are located at positions correspondingly and interact *via* dipole-dipole magnetic interaction:

$$\beta U_{dd} = \frac{\mu_0}{4\pi}\left[\frac{\left(\vec{\mu}(n)\cdot\vec{\mu}(m)\right)}{r_{mn}^3} - \frac{3\left(\vec{\mu}(n)\cdot\vec{r}_{mn}\right)\left(\vec{\mu}(m)\cdot\vec{r}_{mn}\right)}{r_{mn}^5}\right], \quad (2)$$

where, is the vector connecting platelet centres and ; μ_0 is the magnetic vacuum permeability. This interaction favours head-to-tail orientation of dipole moments, which can be additionally enhanced by an applied magnetic field . The latter tends to align any platelet dipole along its direction through Zeeman interaction:

$$\beta U_H = -\mu_0\left(\vec{\mu}\cdot\vec{H}\right). \quad (3)$$

Even though the point dipole approximation might be not fully representative for the magnetisation distribution of platelets shown in Fig. 1, it is a good starting point when investigating diluted systems with relatively strong electrostatic repulsion between platelet surfaces.

We consider electrostatic repulsion between platelets to be strong enough to also prevent Van der Waals aggregation, as seen by the colloidal stability in experiment. The electrostatics itself here is modelled using the screened Coulomb/Debye-Hueckel potential to implicitly account for the electrostatic effects of the ionic strength of the solution, while explicitly incorporating the experimental measurements of electrostatic suspension properties discussed in [66]. Specifically, in addition to the Bjerrum length l_B, the Debye length κ^{-1} is a parameter in the interaction potential:

$$U_{dh} = l_B k_B T \frac{q_1 q_2 e^{-\kappa r}}{r}. \quad (4)$$

Since the entire surface of the platelets should be repulsive, each raspberry bead carries this interaction potential with a charge of $q = Q/n$, where Q is the total platelet charge and n is the number of beads in the platelet.

3.2. General scheme

The equilibrium properties of a system of N MPLs in the cubic volume V at constant temperature T are studied by conducting simulations in the NVT ensemble in a fully 3D periodic system, using the Langevin thermostat [67]. The latter introduces stochastic and friction terms in the translational and rotational Newtonian equations of motion in order to implicitly mimic the effects of the thermal fluctuations of the liquid solvent. Thus, we refrain at this point from simulating hydrodynamic interactions between platelets and only focus on the static structural and magnetic response.

All simulations in this work were performed using the ESPReSso simulation package [68]. This software provides numerous modules, which include CPU parallelised implementations of all the algorithms employed here. Long-range interactions between explicit dipoles in bulk suspensions are computed using periodic boundary conditions and the p^{3}m method, based on fast Fourier transforms of Ewald summations [69]. The latter is based on an efficient approach that splits the magnetic field at a given position into contributions of near and distant dipoles, discretising the positions of the latter into an optimised lattice [70].

The timestep of the simulations is set to $\Delta t = 0.001$. All simulations were initialised by randomly placing $N = 200$ (monodisperse) or $N = 198$ (polydisperse) platelets in a simulation box sized such that the volume density corresponded to 0.04. In the polydisperse simulations, the particle size distribution was chosen by taking the relative frequency of the particle sizes in experiment (shown in Fig. 1(a)), doubling it and rounding to the nearest integer number of particles. The simulation then consists of 3 warmup blocks of 10,000 integrations each. First, a capped block – the upper limit of forces in the system is set to a constant and all forces exceeding this value are reduced to this value – with only steric interactions enabled was run to safely distance overlapping particles. The second step was the introduction of the (initially capped) electrostatic repulsion, then in the final block the cap was removed and the magnetic interactions were enabled. After these warmups had concluded, the external magnetic field was introduced (if applicable) and we began to monitor the system energies. After approximately 60,000 integrations the energy reached a steady fluctuation rate, at which point we began sampling the systems every 5000 integrations. These samples were later used to compute all the results depicted in the figures shown in this paper. Overall, samples were drawn from 92 different simulation (re-)runs with varying field strengths, resulting in 60–300 samples for each system configuration, as *e.g.* the polydisperse zero-field simulations required fewer measurements to produce statistically significant results.

3.3. Dimensionless parameters. Relation to the experiment

Firstly, we should note that all system parameters relevant to the simulation are described by the dimensions of length, time, mass and electric current. We set the reduced length scale by defining $\sigma = 1$ to be one platelet diameter, *i.e.* $l^* = 7$ nm. This already allows us to compute $l_b \approx 0.46$ and $\kappa \approx 0.27$ by plugging in the values obtained in [66] for the suspension of platelets in 1-butanol at a temperature of 25 °C. The remaining three dimensions are fixed by setting the average

magnetic moment $2 \cdot 10^{18}$ Am^2 to 1 (thus fixing the electric current scale), then setting the unit charge $e_0 = 1.602176634 \cdot 10^{19}$ to 1 (fixing the timescale) and finally setting $k_bT = 1$ (fixing the remaining mass scale). This means that we are able to estimate the platelet charge for a given size by using the experimental measurement of the zeta potential [66] and the formula for a sphere of an equivalent size [71], assuming $\psi_s \approx \zeta$:

$$Ze_0 = \frac{4\pi\varepsilon\varepsilon_0\kappa R_{eq}^2 k_B T}{e_0}\left(2\sinh\left(\frac{e_0\psi_s}{2k_BT}\right) + \frac{4}{\kappa R_{eq}}\tanh\left(\frac{e_0\psi_s}{4k_BT}\right)\right)$$

and calculate the magnetic moment of a platelet of a given size by scaling the average moment with the volume of the platelet. The external fields in simulation were set from $H = 0.1$ to $H = 10$, which corresponds to approximately 0.25 to 25 mT. Since these considerations already fit the simulation system to experiment, two remaining potential parameters, the Lennard-Jones well depth ε and the magnetic Bjerrum length, are set to $\varepsilon = k_bT = 1$ and $l_{BM} = 1/(k_BT) = 1$ respectively.

4. Results and discussions

4.1. Zero external field case: intrinsic anisotropy

We start analysing the influence of polydispersity on structural properties by computing centre-to-centre radial distribution functions (RDFs), $g(r)$ [72]. These functions are relevant only for zero field and low density, as only under such condition the system remains disordered. In Fig. 3 one can see that up to roughly 35 nm $g(r)$ is zero, clearly reflecting the weakness of magnetic inter-platelet correlations and the absence of stack formation. We observe that there is a clear preferred spacing between the platelets, at approximately $r = 63$ nm for the monodisperse case. This corresponds to approximately 1.5 platelet diameters. In the polydisperse case, this peak is shifted to a slightly larger separation due to the lognormal size distribution of the platelets, as the average platelet is larger than the median used in the monodisperse case. The first peak for the polydisperse system is lower and broader than its monodisperse counterpart due to the variety of different platelet sizes. The comparison of the second peak, indicating the separation of the next nearest neighbours, shows that for the polydisperse systems this distance is barely pronounced, while it remains prominent for the monodisperse suspensions. This does not, however, imply that the monodisperse system is more correlated. Rather the height differences can be attributed to the combinatoric spread in the distances, which has the outcome of a higher degree of spatial disorder in the polydisperse case.

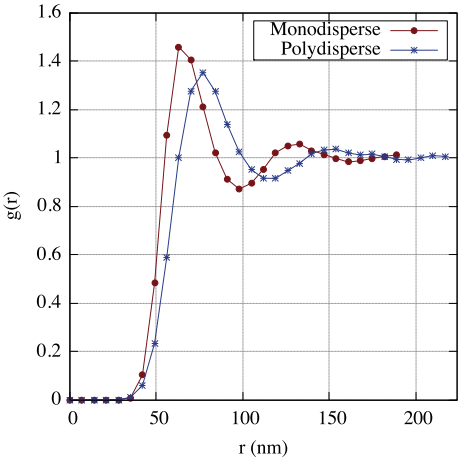

Fig. 3. Zero field isotropic RDFs, $g(r)$, of monodisperse and polydisperse systems: red circles – monodisperse system; blue crosses – polydisperse system. The lines are guides to the eye. Here and below if it is not mentioned explicitly, the size of the simulation symbol is larger than the error-bars.

The radial distribution function is not accessible in experiment, however, small angle X-Ray scattering (SAXS) measurements can provide an insight into the spatial distribution of the platelets in the polydisperse case. An alternative method to investigate the structure of these systems would have been small angle neutron scattering (SANS), as described in Ref. [73] and references therein. The SAXS scattered intensity is proportional to the differential scattering cross section, which for polydisperse interacting colloids can be written as:

$$\frac{d\sigma}{d\Omega}\left(\vec{q}\right) = \frac{N_p}{V}\left\langle\left|F\left(\vec{q},\vec{n}\right)\right|^2\right\rangle + \\ +V^{-1}\left\langle\sum_{i=1}^{N_p}\sum_{i\neq j}F_i\left(\vec{q},\vec{n}_i\right)F_j\left(\vec{q},\vec{n}_j\right)\exp\left(-i\vec{q}\cdot\left(\vec{r}_j-\vec{r}_i\right)\right)\right\rangle. \quad (5)$$

Here, V is the scattering volume, N_p the number of particles within V, the scattering vector, the position and the scattering amplitude of the i-th particle. For particles of anisotropic shape, also depends on the particle's orientation, which is denoted by a unit vector . The brackets ⟨⟩ denote averaging over all possible configuration of the particle's positions and orientations at a given temperature.

In experiment, two suspensions were compared, a diluted one with volume density $c_0 = 0.003$ and more concentrated one with $c_c = 0.04$. They were sealed in rectangular capillaries with dimension 0.05 mm × 1 mm and placed into SAXS instrument (Bruker AXS Nanostar). To obtain zero field conditions, the ambient Earth's magnetic field was cancelled using 3 pairs of coils. The scattered intensity from both suspension was radially symmetric, *i.e.*, it depended only on the modulus of the scattering vector , so radial integration of the scattered intensity was performed to obtain better statistics. In the diluted suspension (0.003), there are no correlations between the platelets, thus the second term in Eq. (5) is zero and the scattered intensity $I(q,c_0)$ is a sum of scattered intensities from individual particles. In this case, the scattering experiment gives information on particles' shape averaged over size and orientation.

$$I(q,c_0) \propto \frac{N_p}{V}\left\langle\left|F\left(\vec{q},\vec{n}\right)\right|^2\right\rangle. \quad (6)$$

In the most concentrated suspension, correlations between particles exist, which can be clearly observed when the scattered intensity from concentrated suspension I(q,c_c)is divided by the scattered intensity from diluted suspension, which yields experimental structure factor defined as

$$\tilde{S}(q) + 1 = \frac{c_0}{c_c} I(q,c_c)/I(q,c_0). \quad (7)$$

In Fig. 4(a) we plot , providing the experimental error-bars. The advantages of using SAXS were also discussed in the context of ferrofluids with spherical nanoparticles in Ref. [74].

One can clearly see that the first peak is very pronounced and its position corresponds to the q ~ 0.35. The second peak is found at twice larger value of q. Even though these values cannot be directly related to real space separations between platelet centres, the overall shape of qualitatively represents the behaviour of the centre-to-centre $S(q)$, available in simulations and described by Eq. (8).

$$S\left(\vec{q}\right) = \frac{1}{N}\sum_{j=1}^{N}\sum_{k=1}^{N} e^{-i\vec{q}\cdot\left(\vec{r}_j-\vec{r}_k\right)}. \quad (8)$$

Here, we have to note that because the particles are anisotropic and polydisperse and because the platelets' orientation and

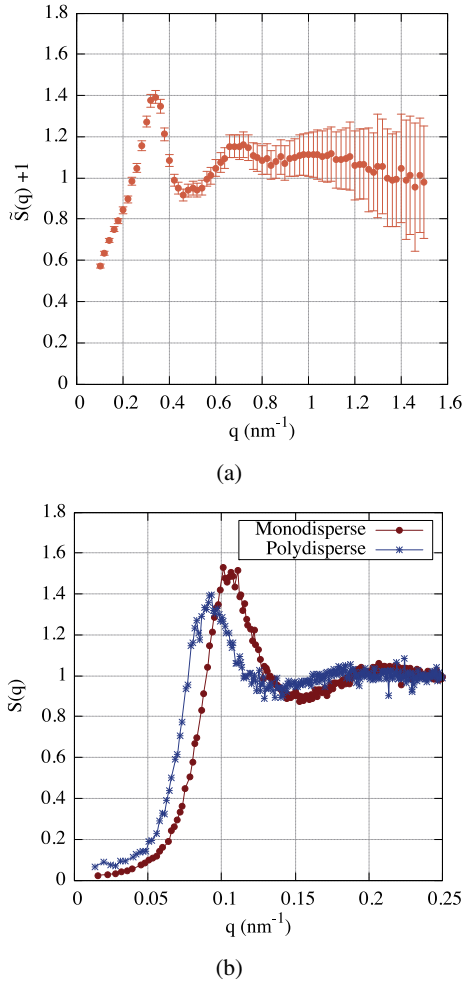

Fig. 4. (a) Experimental data for $+1$ from Eq. (5). (b) Simulation results for the zero-field isotropic SFs, $S(q)$, of monodisperse and polydisperse systems: red circles – monodisperse system; blue crosses – polydisperse system. The lines are guides to the eye.

relative position are correlated, the second term in Eq. (5) cannot be decomposed into a product of the usual structure factor (defined in Eq. (8)) and the square average of the form factor as it is usually done for spherical particles. This is a common issue in interpretation of SAXS or SANS data [73,75,76]. However, when the correlation peaks are distinctive as shown in Fig. 4(a), qualitative comparison of the position of the correlation peaks with the structure function obtained from simulations data is still possible and such analysis is justified. So although a direct comparison would not be fruitful, one finds an excellent agreement in terms of peak height, peak separation and overall shape as shown in Fig. 4(b). The monodisperse case clearly recovers the peak at $2\pi/0.1 \approx 63$ nm and shows a secondary peak at roughly $2\pi/0.2 \approx 31$ nm, which corresponds to the distance where the radial distribution function begins to be non-zero. In the polydisperse case, we also see the peak at slightly greater distances than in the monodisperse case, confirming what was shown by the radial distribution function.

To conclude this section, we can say that the coarse-grained representations adequately describes the system of polydisperse magnetic platelets. Thus, one can conclude that the system's polydispersity leads to an overall spread in the characteristic inter-platelets distances. Moreover, the problems of polydispersity were actively discussed for SANS experiments with conventional ferrofluids containing quasi-spherical nanoparticles [76], so that one can use them in the future investigations. Below, we will use only simulation data to describe in more detail the structure of isotropic phase in the system of poly- and monodisperse nanoplatelets.

4.1.1. Bond-order parameters

In order to quantitatively characterise spatial monomer distribution, we calculate the order parameters for the platelet centres. In order to do that we obtain

$$Q_{lm}\left(\vec{r}_{ij}\right) = Y_{lm}\left(\theta\left(\vec{r}_{ij}\right), \phi\left(\vec{r}_{ij}\right)\right), \tag{9}$$

where Y_{lm} are spherical harmonics of the respective order, lm, and angles θ and ϕ are correspondingly azimuthal and polar angles of a displacement vector between two platelets, in a lab reference frame. Only those pairs of platelets are taken into consideration, whose separation is smaller than the value of the first RDF minimum, as shown in Fig. 4.1. The function is averaged over all such particles, i, j, then over time and, finally, over all runs:

$$\overline{Q}_{lm} = \langle Q_{lm} \rangle. \tag{10}$$

The resulting cumulant bond order parameter Q_l,

$$Q_l = \left[\frac{4\pi}{2l+1}\sum_{m=-l}^{l}\left|\overline{Q}_{lm}\right|^2\right]^{1/2}, \tag{11}$$

is plotted in Fig. 5 in the form of histograms. It is known that based on Q_l distribution, one can distinguish between different crystalline ordering in the system [77].

Looking at this figure, one can see that inherent to crystalline order Q_4 or Q_6 are negligibly small, and that the largest value is obtained by Q_3, which might be attributed to a precursor to a honey-comb-like structure. However, the values of Q_3, not to mention the others, remain very low to reveal a fully liquid state of both mono- and poly-disperse systems. In general, Fig. 5, shows that on the level of nearest neighbours the polydispersity does not affect the relative local structure, rather it contributes to the longer range properties.

4.2. Impact of an applied magnetic field

We applied external fields between $H = 0.1$ ($\approx$0.25 mT, very low) and $H = 10$ ($\approx$25 mT, very high) to the simulated suspensions of monodisperse platelets and analysed both magnetic response and structural transformations.

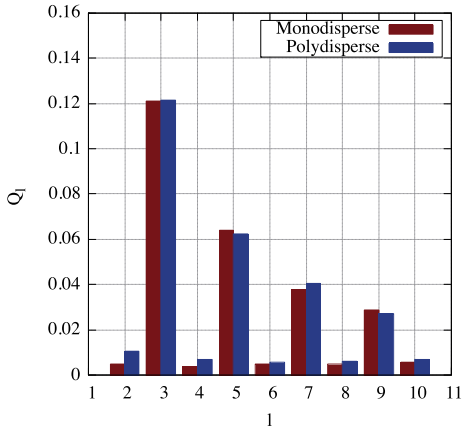

Fig. 5. Bond order parameter Q_l, Eq. (11), as a function of l. Red – monodisperse case; blue–polydisperse system.

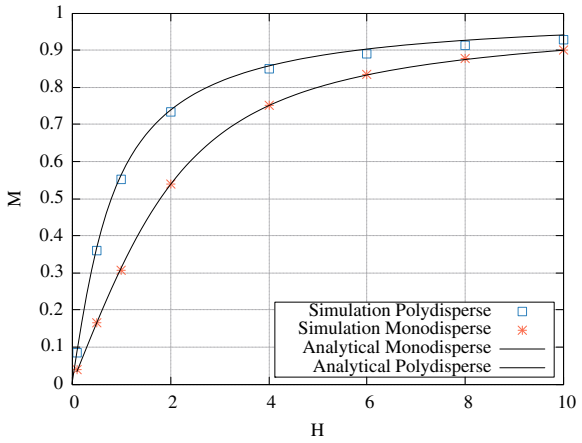

Fig. 6. Magnetisation curves. M and H are in simulation units and therefore dimensionless. Symbols – simulation data, solid lines – predictions of Eqs. (12) and (14) that coincide for both systems. Blue squares are used for the polydisperse system; red stars for the monodisperse case.

4.2.1. Magnetisation curves

The magnetisation M *i.e.* the sum of the projections of all magnetic moments in the system on the field axis shown in Fig. 6 with symbols, is measured for mono- and polydisperse systems in simulation (red and blue lines) and normalised by the value of saturation magnetisation of corresponding systems, M_s, obtained as direct sums of all platelets moments. The lines are the result of two different analytical models. It is well known that the magnetisation M_L of an ideal monodisperse superparamagnetic gas obeys a Langevin law [78,79]:

$$M_L(H) = M_s L\left(\frac{\mu H}{k_B T}\right), \tag{12}$$

where $L(\alpha)$ is the Langevin function:

$$L(\alpha) = \coth(\alpha) - \frac{1}{\alpha}. \tag{13}$$

In case the system is polydisperse, Eq. (12) can be generalised by weighting the integral average with the particle size distribution [80]. Usually, however, magnetic interparticle correlations are very important. A reliable model to take them into account for both mono- and poly-disperse moderately concentrated and non-cluster-forming magnetic systems results from a the so-called modified mean-field theory of the second order (MMFT2) [81]. In the framework of MMFT2, the magnetisation of the system is obtained by replacing H in Eq. (12) by an effective field $H_e(H)$:

$$H_e(H) = H + \frac{1}{3} M_s L\left(\frac{\mu H}{k_B T}\right) + \frac{1}{48} (M_s)^2 L\left(\frac{\mu H}{k_B T}\right) \frac{dL\left(\frac{\mu H}{k_B T}\right)}{dH}. \tag{14}$$

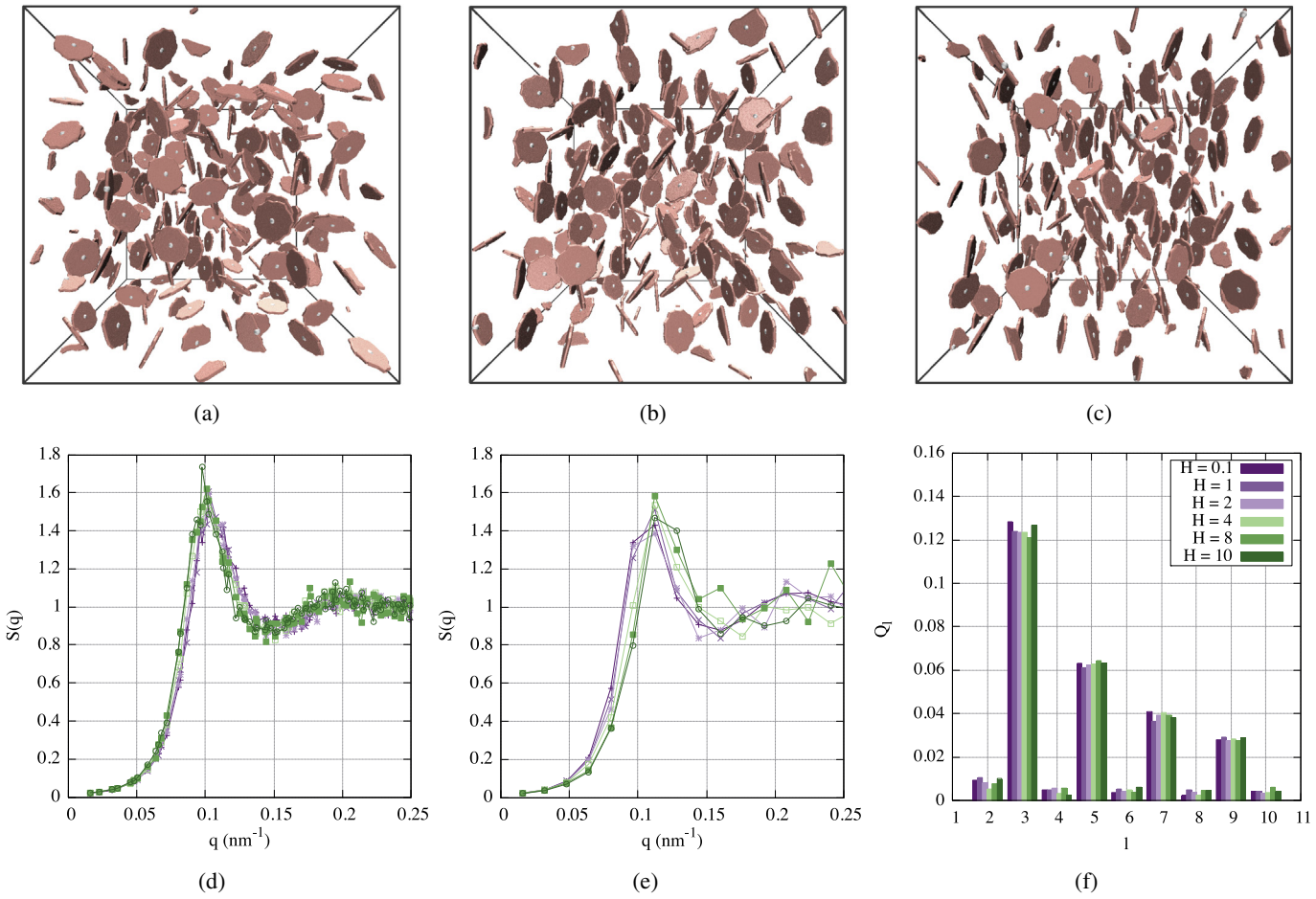

Fig. 7. Structural properties of the monodisperse platelets suspension. Snapshots of the platelet system (a) $H = 2$; (b) $H = 4$; (c) $H = 8$. The field points along x-axis and corresponds to the direction from the left to the right in the figure. (d) Structure factor, $S(q_\perp)$, calculated in the plane perpendicular to the vector of an applied magnetic field, H. (e) Structure factor, $S(q_\parallel)$, calculated along the field direction. (f) Bond order parameters calculated for different fields. The values of the field colour-coding is provided in (f) and is the same for (d) and (e).

Both simulation cases are almost identical to the predictions of MMFT2, that in turn fully coincide with Langevin magnetisation. This suggests that the platelets are fully magnetically uncorrelated. The reason for that is a very strong electrostatic repulsion in combination with a very low number density. As it can be seen in Fig. 6, the polydisperse system has a higher initial slope of $M(H)$, that is the initial susceptibility. This can be attributed to a small fraction of very large, therefore strongly magnetic platelets in the polydisperse system. Once the structure of the monodisperse system has been analysed in detail, we show how this fraction of platelets actually affects the overall field-induced anisotropy in the suspension.

4.2.2. Field-induced structural anisotropy

In this section we investigate the impact of an applied external magnetic field on the structural properties of both poly- and monodisperse systems. As we expect the system to become spatially anisotropic under the influence of the external field, H, we decided to calculate centre-to-centre structure factors parallel and perpendicular to the direction of H. This is done by splitting $\vec{q}$ into two components $q_\perp = \left|\vec{q}_\perp\right| = \left|\left(0, q_y, q_z\right)\right|$ and $q_\parallel = \left|\vec{q}_\parallel\right| = |(q_x, 0, 0)|$.

In Fig. 7, we plot a set of simulation snapshots for a selection of fields. Examining the snapshots (a) through (c), we see that the system remains completely isotropic for low fields, then, as the field goes above $H = 2$, begins to exhibit faint signs of orientational preference to align with the field, and appears strongly aligned once H grows to 8. However, the ordering in Fig. 7(c) is far from being perfect.

This is reflected in the structure factor perpendicular to the field, which appears nearly identical to that of the zero-field suspension for fields lower than $H = 2$ (in purple), then shifts to larger distances as the field grows large (in green), Fig. 7(d). The opposite trend can be observed for the structure factor parallel to the field, which is initially identical to that perpendicular to the field, then shifts to nearer distances as the field grows: one observes a light shift of the first peak position to the right (compare purple and green curves in Fig. 7(e)). Overall, the characteristic separation found in the field-free case is conserved up to fields of approximately $H = 2$: after this, the characteristic distance splits into a characteristic short separation parallel to the field and larger separation perpendicular as a nematic-like ordering of the platelets is induced by the external field. It should again be remarked that this is mirrored by the alignment of the platelets with the field, and we only consider center-to-center distances, which means that the minimum separation between platelets that may come to lie in plane would have to be at least a platelet diameter. This not a sharp transition taking place at a specific field strength: one can see by observing *e.g.* the peak heights for a field of $H = 1$ and $H = 2$ that the increased ordering of the platelets doesn't perfectly correspond to the field strength. Rather, there is an intermediate regime with partial orientational and no positional ordering when the field strength is comparable to the dipole moment. Examining the bond order parameter in Fig. 7(f), we see that the platelets do not adapt any specific ordering as all values are below $Q_l = 0.5$. However, there is a distinct preference for the bond order of 3 across all field strengths, providing an indication that the system may be cultivating a honeycomb structure that already manifests itself for $H = 0$. Indications of this can also be seen by analysis of the simulation snapshots. Concluding that platelets form a honeycomb structure would however be premature, as the bond order parameters are of such low values that they are strongly affected by the noise of the gradual transition seen in Fig. 7(e) in particular.

In the polydisperse case, shown in Fig. 8, we see a much more pronounced shift occurring as soon as the field grows greater than the median dipole moment, $H = 1$. For $H = 2$ in Fig. 8(a) some platelets seem to be already aligned with the field H. If one compares Figs. 7(b) and 8(b), in which $H = 4$, it is easy to notice that even a small fraction of highly anisotropic large diameter platelets is sufficient to induce much higher ordering than it is found in a monodisperse case. The fact that large platelets have higher magnetic moments make them more susceptible to weak fields. At the same time, their high anisotropy once they are aligned with the field perturbs the complete system in a more drastic way. Thus in combination with the external field, the polydisperse system supports an earlier and more pronounced induced nematic-like ordering. For $H = 8$, as shown in Fig. 8(c), the suspension of polydisperse platelets seem to be highly orientationally ordered.

In the structure factor perpendicular to the applied field, Fig. 8(d), the stronger ordering is reflected by a larger shift of the first peak into the region of smaller q, without the added noise of the monodisperse case. Again, we observe an initially isotropic structure factor at very low fields, which splits into a distinct lower separation parallel and greater separation perpendicular (see, Fig. 8(e)) to the field. The orientational ordering could theoretically be accompanied by spatial ordering of the platelets centres. Looking at Fig. 8(f), where we plot the bond order parameters, we again see the tendency towards a honeycomb-like structure which again appears uncorrelated with the field. In other words, orientational ordering caused by the presence of the low fraction of large platelets leads to a more notable evolution of the structure factor both parallel and perpendicular to the applied magnetic field, but does not cause any spatial ordering of platelets centres.

5. Conclusion

We have developed a coarse-grained molecular dynamics model which can qualitatively reproduce the experimental system for low densities and captures the structure of the fluid within reasonable expectation. The developed approach was applied to investigate the structure and the magnetic response of magnetic platelets as well as to elucidate the impact of polydispersity.

We have found that in the absence of an applied magnetic field both poly- and monodisperse systems are in a liquid state with a preferred separation between platelets of approximately one and a half diameters. In the polydisperse case, the characteristic separations have a wider distribution that results in an overall less correlated system. These results are confirmed by SAXS measurements.

This correspondence changes drastically once the magnetic field is applied. Due to the presence of a small fraction of relatively large, highly anisotropic and strongly magnetic platelets in the polydisperse suspension, weak fields already lead to a significant nematic-like ordering in the system. In the monodisperse case the platelets also orient themselves, but the application of a much stronger magnetic field is required. We calculated partial structure factors parallel and perpendicular to the field. For both poly- and mono-disperse systems we observed that for a strong enough field, the characteristic distances in the plane perpendicular to the field increase, whereas those along the field get shorter. This splits the characteristic separation between platelets into a component parallel and perpendicular case, the former of which allows for a closer approach on average, which is promising considering the platelets are expected to stack at higher densities and form a ferromagnetic phase [60].

The analysis of bond order parameters has not revealed any pronounced structuring of the platelets centres. However, we observe a precursor of a discotic honeycomb structure, which can be enhanced by the external field.

Currently, we are focused on the investigations of more concentrated suspensions, aiming at describing the emergence of the ordered phase in the absence of an applied field.

CRediT authorship contribution statement

Margaret Rosenberg: Methodology, Investigation, Formal analysis, Writing - original draft. **Žiga Gregorin:** Investigation. **Patricija Hribar Boštjančič:** Investigation. **Nerea Sebastián:** Investigation, Writing - original draft. **Darja Lisjak:** Investigation. **Sofia S. Kantorovich:** Investigation, Formal analysis, Visualization, Writing - original draft. **Alenka**

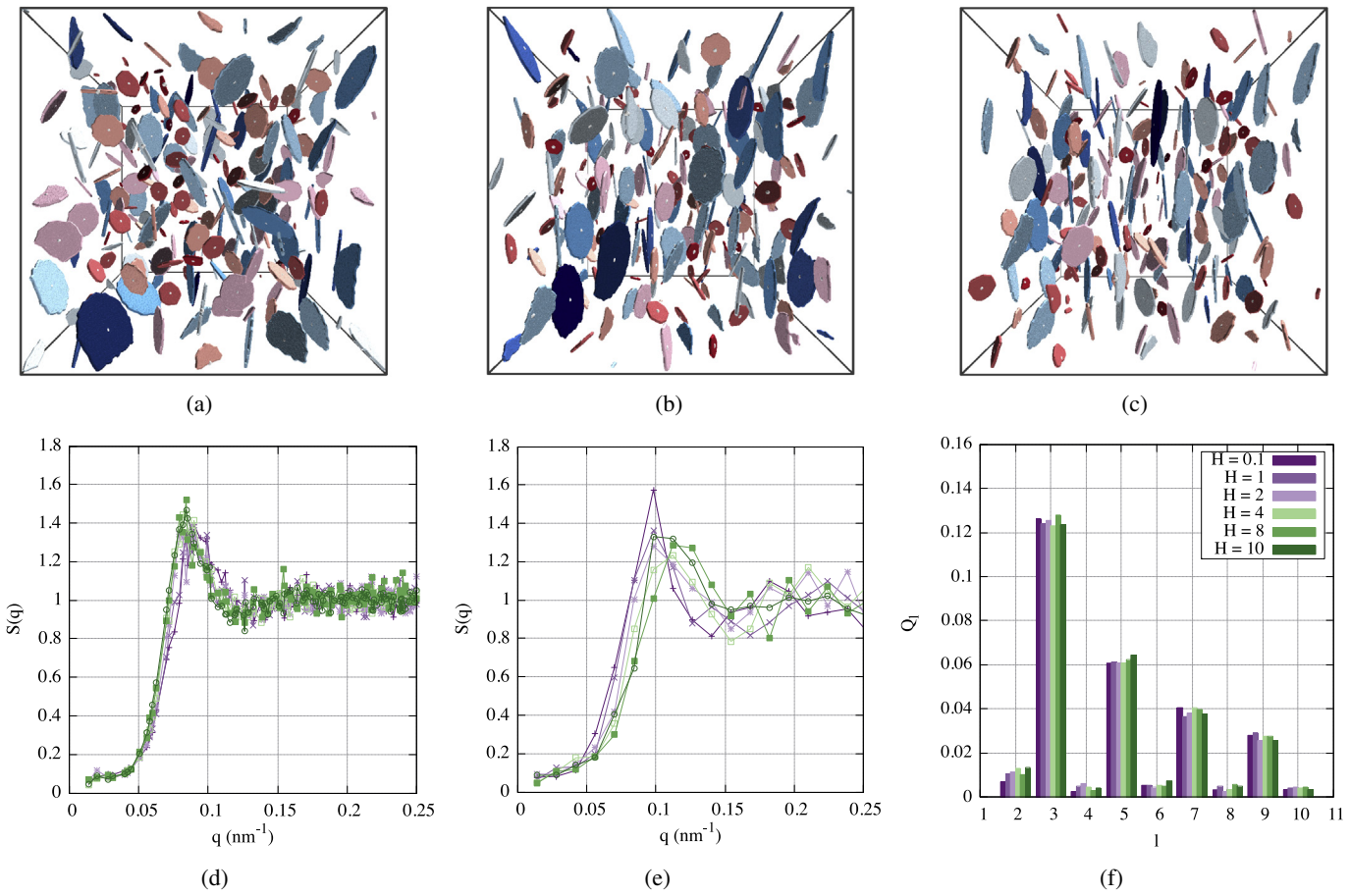

Fig. 8. Structural properties of the polydisperse platelets suspension. Snapshots of the platelet system (a) $H = 2$; (b) $H = 4$; (c) $H = 8$. The field points along x-axis and corresponds to the direction from the left to the right in the figure. (d) Structure factor, $S(q_\perp)$, calculated in the plane perpendicular to the vector of an applied magnetic field, H. (e) Structure factor, $S(q_\parallel)$, calculated along the field direction. (f) Bond order parameters calculated for different fields. The values of the field colour-coding is provided in (f) and is the same for (d) and (e).

Mertelj: Conceptualization, Investigation, Writing - original draft. **Pedro A. Sánchez:** Conceptualization, Software, Writing - original draft.

Declaration of competing interest

There are no conflicts of interest.

Acknowledgments

This research has been supported by the Russian Science Foundation Grant 19-12-00209. The work was also supported by the FWF START-Projekt AY 627-N27. Simulations were performed in Vienna Scientific Cluster (VSC3 and VSC4). NS, DL, ŽG and AM acknowledge the financial support from the Slovenian Research Agency (research core funding P1-0192 and P2-0089 and the project J7-8267). Also, the financial support from OeAD and the Slovenian Research Agency for a bilateral project (WTZ grant number SI 13/2016 and ARRS grant number BI-AT/18-19-009) is acknowledged. We acknowledge support by Prof. H. Peterlik and the Faculty center for Nano Structure Research at the University of Vienna for the assistance with the SAXS measurements and for the use of Bruker AXS Nanostar. We also thank Ekaterina Novak for assistance with the calculation of bond order parameters.

References

[1] S. Odenbach, Ferrofluids: Magnetically Controllable Fluids and Their Applications, Springer, 2011, ISBN 978-3-642-07882-8.

[2] M.A. Khairul, E. Doroodchi, R. Azizian, B. Moghtaderi, Advanced applications of tunable ferrofluids in energy systems and energy harvesters: a critical review, Energy Convers. Manag. 149 (2017) 660–674, https://doi.org/10.1016/j.enconman.2017.07.064 (ISSN 0196-8904).

[3] M.-L. Seol, S.-B. Jeon, J.-W. Han, Y.-K. Choi, Ferrofluid-based triboelectric-electromagnetic hybrid generator for sensitive and sustainable vibration energy harvesting, Nano Energy 31 (2017) 233–238, https://doi.org/10.1016/j.nanoen.2016.11.038 (ISSN 2211-2855).

[4] H.R. Yun, D.J. Lee, J.R. Youn, Y.S. Song, Ferrohydrodynamic energy harvesting based on air droplet movement, Nano Energy 11 (2015) 171–178, https://doi.org/10.1016/j.nanoen.2014.10.023 (ISSN 2211-2855).

[5] A. Bibo, R. Masana, A. King, G. Li, M. Daqaq, Electromagnetic ferrofluid-based energy harvester, Phys. Lett. A 376 (32) (2012) 2163–2166, https://doi.org/10.1016/J.PHYSLETA.2012.05.033 (ISSN 0375-9601).

[6] D. Wang, S. Zheng, H. Liu, J. Tang, W. Miao, H. Wang, Y. Tian, H. Yang, L. Jiang, A magnetic gated nanofluidic based on the integration of a superhydrophilic nanochannels and a reconfigurable ferrofluid, Adv. Mater. 31 (7) (2019) 1805953, https://doi.org/10.1002/adma.201805953 (ISSN 1521-4095).

[7] R.-J. Yang, H.-H. Hou, Y.-N. Wang, L.-M. Fu, Micro-magnetofluidics in microfluidic systems: a review, Sens. Actuators B Chem. 224 (2016) 1–15, https://doi.org/10.1016/J.SNB.2015.10.053 (ISSN 0925-4005).

[8] A.A. Eliseev, A.A. Eliseev, L.A. Trusov, A.P. Chumakov, P. Boesecke, E.O. Anokhin, A.V. Vasiliev, A.E. Sleptsova, E.A. Gorbachev, V.V. Korolev, P.E. Kazin, Rotational dynamics of colloidal hexaferrite nanoplates, Appl. Phys. Lett. 113 (11) (2018) 113106, https://doi.org/10.1063/1.5044728 (ISSN 0003-6951).

[9] X. Zhang, L. Sun, Y. Yu, Y. Zhao, Flexible ferrofluids: design and applications, Adv. Mater. 31 (51) (2019) 1903497, https://doi.org/10.1002/adma.201903497 (ISSN 1521-4095).

[10] K. Ulbrich, K. Holá, V. Šubr, A. Bakandritsos, J. Tuček, R. Zbořil, Targeted drug delivery with polymers and magnetic nanoparticles: covalent and noncovalent approaches, release control, and clinical studies, Chem. Rev. 116 (9) (2016) 5338–5431, https://doi.org/10.1021/acs.chemrev.5b00589 (ISSN 0009-2665).

[11] P. Medle Rupnik, D. Lisjak, M. Čopič, A. Mertelj, Ferromagnetic liquid crystals for magnetic field visualisation, Liq. Cryst. 42 (12) (2015) 1684–1688, https://doi.org/10.1080/02678292.2015.1049570 (ISSN 0267-8292).

[12] H. Takezoe, Polar liquid crystals – ferro, antiferro, banana, and columnar, Mol. Cryst. Liq. Cryst. 646 (1) (2017) 46–65, https://doi.org/10.1080/15421406.2017.1284377 (ISSN 1542-1406).
[13] L.R. Jr, R.E. Rosensweig, Magnetocaloric power, J. AIAA 2 (1964) 1418–1422.
[14] A. Cebers, Thermodynamic stability of magnetic liquids, Magnitnaya Gidrodinamika (in Russ.) 18 (1982) 42.
[15] K. Sano, M. Doi, Theory of agglomeration of ferromagnetic particles in magnetic fluids, J. Phys. Soc. Jpn. 52 (8) (1983) 2810–2815, https://doi.org/10.1143/JPSJ.52.2810.
[16] D. Wei, G. Patey, Orientational order in simple dipolar liquids: computer simulation of a ferroelectric nematic phase, Phys. Rev. Lett. 68 (13) (1992) 2043, https://doi.org/10.1103/PhysRevLett.68.2043.
[17] J.J. Weis, D. Levesque, Chain formation in low density dipolar hard shperes: a Monte Carlo study, Phys. Rev. Lett. 71 (17) (1993 a) 2729–2732.
[18] J.J. Weis, D. Levesque, Ferroelectric phases of dipolar hard shperes, Phys. Rev. E 48 (5) (1993 b) 3728–3740.
[19] B. Groh, S. Dietrich, Long-ranged orientational order in dipolar fluids, Phys. Rev. Lett. 72 (15) (1994 a) 2422, https://doi.org/10.1103/PhysRevLett.72.2422.
[20] B. Groh, S. Dietrich, Ferroelectric phase in Stockmayer fluids, Phys. Rev. E 50 (5) (1994 b) 3814, https://doi.org/10.1103/PhysRevE.50.3814.
[21] G. Ayton, M. Gingras, G. Patey, Orientational ordering in spatially disordered dipolar systems, Phys. Rev. Lett. 75 (12) (1995) 2360, https://doi.org/10.1103/PhysRevLett.75.2360.
[22] B. Groh, S. Dietrich, Structural and thermal properties of orientationally ordered dipolar fluids, Phys. Rev. E 53 (3) (1996) 2509, https://doi.org/10.1103/PhysRevE.53.2509.
[23] B. Groh, S. Dietrich, Inhomogeneous magnetization in dipolar ferromagnetic liquids, Phys. Rev. E 57 (4) (1998) 4535, https://doi.org/10.1103/PhysRevE.57.4535.
[24] S. Klapp, F. Forstmann, Phase behavior of aligned dipolar hard spheres: integral equations and density functional results, Phys. Rev. E 60 (3) (1999) 3183, https://doi.org/10.1103/PhysRevE.60.3183.
[25] H. Mamiya, I. Nakatani, T. Furubayashi, Phase transitions of iron-nitride magnetic fluids, Phys. Rev. Lett. 84 (2000) 6106–6109, https://doi.org/10.1103/PhysRevLett.84.6106.
[26] G. Gao, X.C. Zeng, Freezing transition of a strongly dipolar simple fluid, Phys. Rev. E 61 (3) (2000) R2188, https://doi.org/10.1103/PhysRevE.61.R2188.
[27] A.O. Ivanov, Spontaneous ferromagnetic ordering in magnetic fluids, Phys. Rev. E 68 (2003), 011503. https://doi.org/10.1103/PhysRevE.68.011503.
[28] C. Joslin, Second virial coefficients for a fluid of dipolar hard ellipsoids, Mol. Phys. 47 (4) (1982) 771–783, https://doi.org/10.1080/00268978200100582.
[29] M. Baus, J.-L. Colot, Ferroelectric nematic liquid-crystal phases of dipolar hard ellipsoids, Phys. Rev. A 40 (1989) 5444–5446, https://doi.org/10.1103/PhysRevA.40.5444.
[30] A. Perera, G.N. Patey, Fluids of dipolar hard ellipsoids: structural properties and isotropic–nematic phase transitions, J. Chem. Phys. 91 (5) (1989) 3045–3055, https://doi.org/10.1063/1.456926.
[31] J.M. Caillol, J.J. Weis, Nematic to smectic-a transition of parallel dipolar hard spherocylinders and ellipsoids, a hypernetted chain equation study, J. Chem. Phys. 92 (5) (1990) 3197–3205, https://doi.org/10.1063/1.457870.
[32] G. Zarragoicoechea, D. Levesque, J. Weis, Monte Carlo study of dipolar ellipsoids. II. Search for an isotropic-nematic phase transition, Mol. Phys. 75 (5) (1992) 989–998, https://doi.org/10.1080/00268979200100771.
[33] C. Vega, S. Lago, Isotropic-nematic transition of hard polar and nonpolar molecules, J. Chem. Phys. 100 (9) (1994) 6727–6737, https://doi.org/10.1063/1.467033.
[34] K. Satoh, S. Mita, S. Kondo, Monte Carlo simulations using the dipolar Gay-Berne model: effect of terminal dipole moment on mesophase formation, Chem. Phys. Lett. 255 (1–3) (1996 a) 99–104, https://doi.org/10.1016/0009-2614(96)00355-7 (ISSN 0009-2614).
[35] K. Satoh, S. Mita, S. Kondo, Monte Carlo simulations on mesophase formation using dipolar Gay-Berne model, Liq. Cryst. 20 (6) (1996 b) 757–763, https://doi.org/10.1080/02678299608033169.
[36] K. Satoh, S. Mita, S. Kondo, Influence of longitudinal dipole on mesophase formation via computer simulation, Mol. Cryst. Liq. Cryst. Sci. Tech. Mol. Cryst. Liq. Cryst. 300 (1997) 143–161, https://doi.org/10.1080/10587259708042344.
[37] B. Groh, S. Dietrich, Orientational order in dipolar fluids consisting of nonspherical hard particles, Phys. Rev. E 55 (1997) 2892–2901, https://doi.org/10.1103/PhysRevE.55.2892.
[38] G. Ayton, D.Q. Wei, G.N. Patey, Liquid crystal phases of dipolar discotic particles, Phys. Rev. E 55 (1997) 447–454, https://doi.org/10.1103/PhysRevE.55.447.
[39] S.C. McGrother, A. Gil-Villegas, G. Jackson, The effect of dipolar interactions on the liquid crystalline phase transitions of hard spherocylinders with central longitudinal dipoles, Mol. Phys. 95 (3) (1998) 657–673, https://doi.org/10.1080/00268979809483199.
[40] J.C. Shelley, G.N. Patey, D. Levesque, J.J. Weis, Liquid-vapor coexistence in fluids of dipolar hard dumbbells and spherocylinders, Phys. Rev. E 59 (1999) 3065–3070, https://doi.org/10.1103/PhysRevE.59.3065.
[41] G. Rickayzen, A model dipolar ellipsoidal fluid, Mol. Phys. 98 (10) (2000) 683–692, https://doi.org/10.1080/00268970009483336.
[42] S. Varga, I. Szalai, J. Liszi, G. Jackson, A study of orientational ordering in a fluid of dipolar Gay–Berne molecules using density-functional theory, J. Chem. Phys. 116 (20) (2002) 9107–9119, https://doi.org/10.1063/1.1469607.
[43] A. Malijevsky, G. Jackson, S. Varga, Many-fluid Onsager density functional theories for orientational ordering in mixtures of anisotropic hard-body fluids, J. Chem. Phys. 129144504 (14) (2008)https://doi.org/10.1063/1.2982501.
[44] J. Sánchez, C. Rinaldi, Magnetoviscosity of dilute suspensions of magnetic ellipsoids obtained through rotational Brownian dynamics simulations, J. Colloid Interface Sci. 331 (2) (2009) 500–506, https://doi.org/10.1016/j.jcis.2008.11.061 (ISSN 0021-9797).
[45] S.C. McGrother, G. Jackson, Island of vapor-liquid coexistence in dipolar hard-core systems, Phys. Rev. Lett. 76 (1996) 4183–4186, https://doi.org/10.1103/PhysRevLett.76.4183.
[46] L. Rovigatti, J. Russo, F. Sciortino, No evidence of gas-liquid coexistence in dipolar hard spheres, Phys. Rev. Lett. 107 (2011), 237801. https://doi.org/10.1103/PhysRevLett.107.237801.
[47] S. Kantorovich, E. Pyanzina, C. De Michele, F. Sciortino, How to calculate structure factors of self-assembling anisotropic particles, Soft Matter 9 (2013) 4412–4427, https://doi.org/10.1039/C3SM27895F.
[48] D. Levesque, J.J. Weis, G.J. Zarragoicoechea, Monte Carlo simulation study of mesophase formation in dipolar spherocylinders, Phys. Rev. E 47 (1993) 496–505, https://doi.org/10.1103/PhysRevE.47.496.
[49] E. Gwozdz, A. Brodka, K. Pasterny, Molecular dynamics simulation study of a liquid crystal model: Gay-Berne particles with transverse dipole moments, Chem. Phys. Lett. 267 (5) (1997) 557–562, https://doi.org/10.1016/S0009-2614(97)00147-4.
[50] A. Gil-Villegas, S.C. McGrother, G. Jackson, Chain and ring structures in smectic phases of molecules with transverse dipoles, Chem. Phys. Lett. 269 (5) (1997) 441–447.
[51] R. Berardi, S. Orlandi, C. Zannoni, Monte Carlo simulations of rod-like Gay-Berne mesogenes with transverse dipoles, Int. J. Mod. Phys. C 10 (02n03) (1999) 477–484, https://doi.org/10.1142/S012918319900036X.
[52] R. Berardi, S. Orlandi, C. Zannoni, Columnar phases and field induced biaxiality of a Gay-Berne discotic liquid crystal, Phys. Chem. Chem. Phys. 2 (2000) 2933–2942, https://doi.org/10.1039/B001604G.
[53] T.K. Bose, J. Saha, Origin of tilted-phase generation in systems of ellipsoidal molecules with dipolar interactions, Phys. Rev. E 86 (2012), 050701. https://doi.org/10.1103/PhysRevE.86.050701.
[54] S. Sacanna, L. Rossi, B.W.M. Kuipers, A.P. Philipse, Fluorescent monodisperse silica ellipsoids for optical rotational diffusion studies, Langmuir 22 (4) (2006) 1822–1827, https://doi.org/10.1021/la052484o.
[55] M. Nakade, T. Ikeda, M. Ogawa, Synthesis and properties of ellipsoidal hematite/silicone core-shell particles, J. Mater. Sci. 42 (2007) 4815–4823, https://doi.org/10.1007/s10853-006-0761-9 (ISSN 0022-2461).
[56] S.C. McGrother, A. Gil-Villegas, G. Jackson, The liquid-crystalline phase behaviour of hard spherocylinders with terminal point dipoles, J. Phys. Cond. Matter 8 (47) (1996) 9649, https://doi.org/10.1088/0953-8984/8/47/078.
[57] H.N.W. Lekkerkerker, F.M. van der Kooij, K. Kassapidou, Liquid crystal phase transitions in suspensions of polydisperse plate-like particles, Nature 406 (6798) (2000) 868–871, https://doi.org/10.1038/35022535 (ISSN 00280836).
[58] D. Van Der Beek, A.V. Petukhov, P. Davidson, J. Ferré, J.P. Jamet, H.H. Wensink, G.J. Vroege, W. Bras, H.N. Lekkerkerker, Magnetic-field-induced orientational order in the isotropic phase of hard colloidal platelets, Phys. Rev. E 73 (4) (2006) 41402, https://doi.org/10.1103/PhysRevE.73.041402 (ISSN 15393755).
[59] P. Davidson, C. Penisson, D. Constantin, J.-C.P. Gabriel, Isotropic, nematic, and lamellar phases in colloidal suspensions of nanosheets, PNAS (2018) 1091–6490, https://doi.org/10.1073/pnas.1802692115 (201802692, ISSN 0027-8424).
[60] M. Shuai, A. Klittnick, Y. Shen, G.P. Smith, M.R. Tuchband, C. Zhu, R.G. Petschek, A. Mertelj, D. Lisjak, M. Čopič, J.E. Maclennan, M.A. Glaser, N.A. Clark, Spontaneous liquid crystal and ferromagnetic ordering of colloidal magnetic nanoplates, Nat. Commun. 7 (2016) 10394, https://doi.org/10.1038/ncomms10394 (ISSN 2041-1723).
[61] B. Huke, M. Lücke, Magnetic properties of colloidal suspensions of interacting magnetic particles, Rep. Prog. Phys. 67 (10) (2004) 1731–1768, https://doi.org/10.1088/0034-4885/67/10/R01 (ISSN 0034-4885).
[62] A. Hubert, R. Schäfer, Magnetic Domains the Analysis of Magnetic Microstructures, Springer Berlin, 2014.
[63] M. Drofenik, M. Kristl, A. Žnidaršič, D. Hanžel, D. Lisjak, Hydrothermal synthesis of Ba-hexaferrite nanoparticles, J. Am. Ceram. Soc. 90 (7) (2007) 2057–2061, https://doi.org/10.1111/j.1551-2916.2007.01740.x (ISSN 0002-7820).
[64] D. Lisjak, M. Drofenik, Chemical substitution—an alternative strategy for controlling the particle size of barium ferrite, Cryst. Growth Des. 12 (11) (2012) 5174–5179, https://doi.org/10.1021/cg301227r (ISSN 1528-7483).
[65] J.D. Weeks, D. Chandler, H.C. Andersen, Role of repulsive forces in determining the equilibrium structure of simple liquids, J. Chem. Phys. 54 (1971) 5237.
[66] P. Hribar Boštjančič, M. Tomšič, A. Jamnik, D. Lisjak, A. Mertelj, Electrostatic interactions between barium hexaferrite nanoplatelets in alcohol suspensions, J. Phys. Chem. C 123 (37) (2019) 23272–23279, https://doi.org/10.1021/acs.jpcc.9b07455 (ISSN 1932-7447).
[67] D. Frenkel, B. Smit, Understanding Molecular Simulation, Academic Press, 2002.
[68] F. Weik, R. Weeber, K. Szuttor, K. Breitsprecher, J. de Graaf, M. Kuron, J. Landsgesell, H. Menke, D. Sean, C. Holm, ESPResSo 4.0 – an extensible software package for simulating soft matter systems, Eur. Phys. J. ST 227 (14) (2019) 1789–1816, https://doi.org/10.1140/epjst/e2019-800186-9.
[69] A.Y. Toukmaji, J.A. Board, Ewald summation techniques in perspective: a survey, Comput. Phys. Commun. 95 (2) (1996) 73–92, https://doi.org/10.1016/0010-4655(96)00016-1.
[70] J.J. Cerdà, V. Ballenegger, O. Lenz, C. Holm, P3M algorithm for dipolar interactions, J. Chem. Phys. 129 (2008), 234104. https://doi.org/10.1063/1.3000389.
[71] D.A.S.W.R. Russel, B. Saville, Colloidal Dispersions, Cambridge University Press, 1992.
[72] B. Smith, D. Frenkel, Understanding Molecular Simulations, Academic, New York, 1996.
[73] M. Avdeev, V. Aksenov, M. Balasoiu, V. Garamus, A. Schreyer, G. Tőrők, L. Rosta, D. Bica, L. Vékás, Comparative analysis of the structure of sterically stabilized ferrofluids on polar carriers by small-angle neutron scattering, J. Colloid Interface

Sci. 295 (1) (2006) 100–107, https://doi.org/10.1016/j.jcis.2005.07.048 , URL http://www.sciencedirect.com/science/article/pii/S002197970500812X (ISSN 0021-9797).
[74] A. Veligzhanin, D. Frey, A. Shulenina, A. Gruzinov, Y. Zubavichus, M. Avdeev, Characterization of aggregate state of polydisperse ferrofluids: some aspects of anisotropy analysis of 2D SAXS in magnetic field, J. Magn. Magn. Mater. 459 (2018) 285–289, https://doi.org/10.1016/j.jmmm.2017.10.052 , URL http://www.sciencedirect.com/science/article/pii/S0304885317320681 (ISSN 0304-8853, the selected papers of Seventh Moscow International Symposium on Magnetism (MISM-2017)).
[75] M. Kotlarchyk, S.-H. Chen, Analysis of small angle neutron scattering spectra from polydisperse interacting colloids, J. Chem. Phys. 79 (5) (1983) 2461–2469, https://doi.org/10.1063/1.446055.
[76] M.V. Avdeev, Particle interaction in polydisperse magnetic fluids: experimental aspects of small-angle neutron scattering applications, J. Mol. Liq. 189 (2014) 68–73, https://doi.org/10.1016/j.molliq.2013.05.019 , URL http://www.sciencedirect.com/science/article/pii/S0167732213001906 (ISSN 0167-7322, fluid phase associations).
[77] P.J. Steinhardt, D.R. Nelson, M. Ronchetti, Bond-orientational order in liquids and glasses, Phys. Rev. B 28 (1983) 784–805, https://doi.org/10.1103/PhysRevB.28.784.
[78] P. Langevin, Sur la theory du magnetism, J. de Phys. 4 (1905 a) 678.
[79] P. Langevin, Magnetism et theory des electrons, Ann. Chim. et Phys. 5 (1905 b) 70.
[80] A. Ivanov, S. Kantorovich, E. Reznikov, C. Holm, A. Pshenichnikov, A.A. Chremos, P. Camp, Magnetic properties of polydisperse ferrofluids: a critical comparison between experiment, theory and computer simulation, Phys. Rev. E 75 (2007) 61405.
[81] A.O. Ivanov, O.B. Kuznetsova, Magnetic properties of dense ferrofluids: an influence of interparticle correlations, Phys. Rev. E 64 (2001), 041405. https://doi.org/10.1103/PhysRevE.64.041405.